Supplemental Materials

Molecular Biology of the Cell

Bastounis et al.

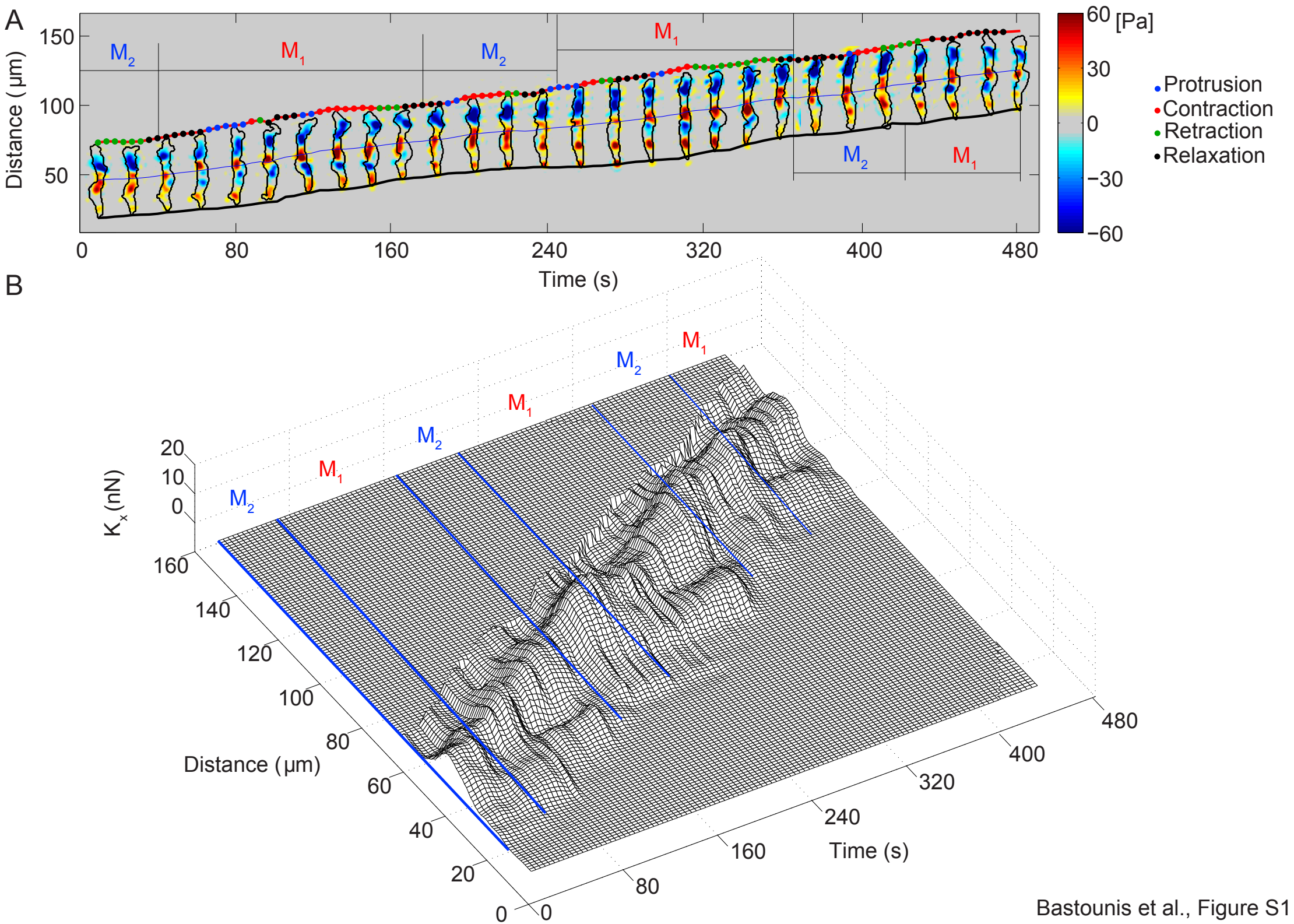

Bastounis et al., Figure S1

A

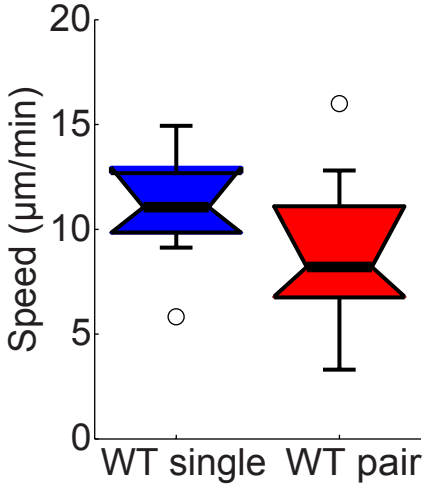

B

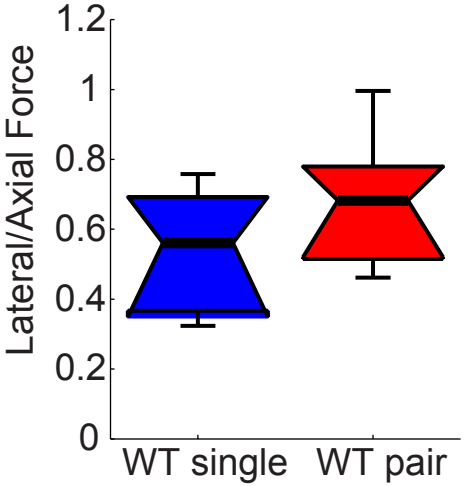

C

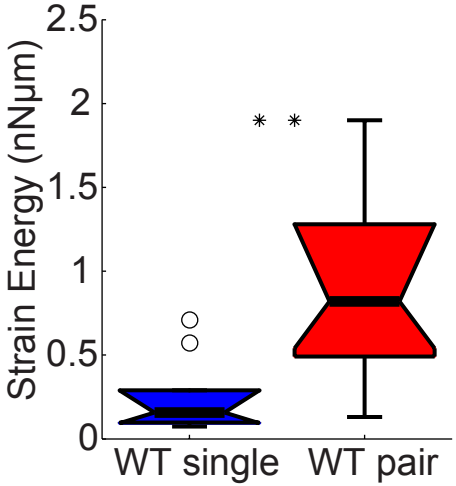

D

# of cells/ Mode	V (μm/min)	U_s (nNμm)	F_y/F_x
Single cell (N=12)	11.07+/-2.36	0.23+/-0.20	0.54+/-0.16
Streaming cell pair/ M1 (N=14)	9.02+/-3.39	0.89+/-0.42	0.66+/-0.15
Streaming cell pair/ M2 (N=14)	7.66+/-4.06	1.19+/-0.76	0.69+/-0.17

Bastounis et al., Figure S2

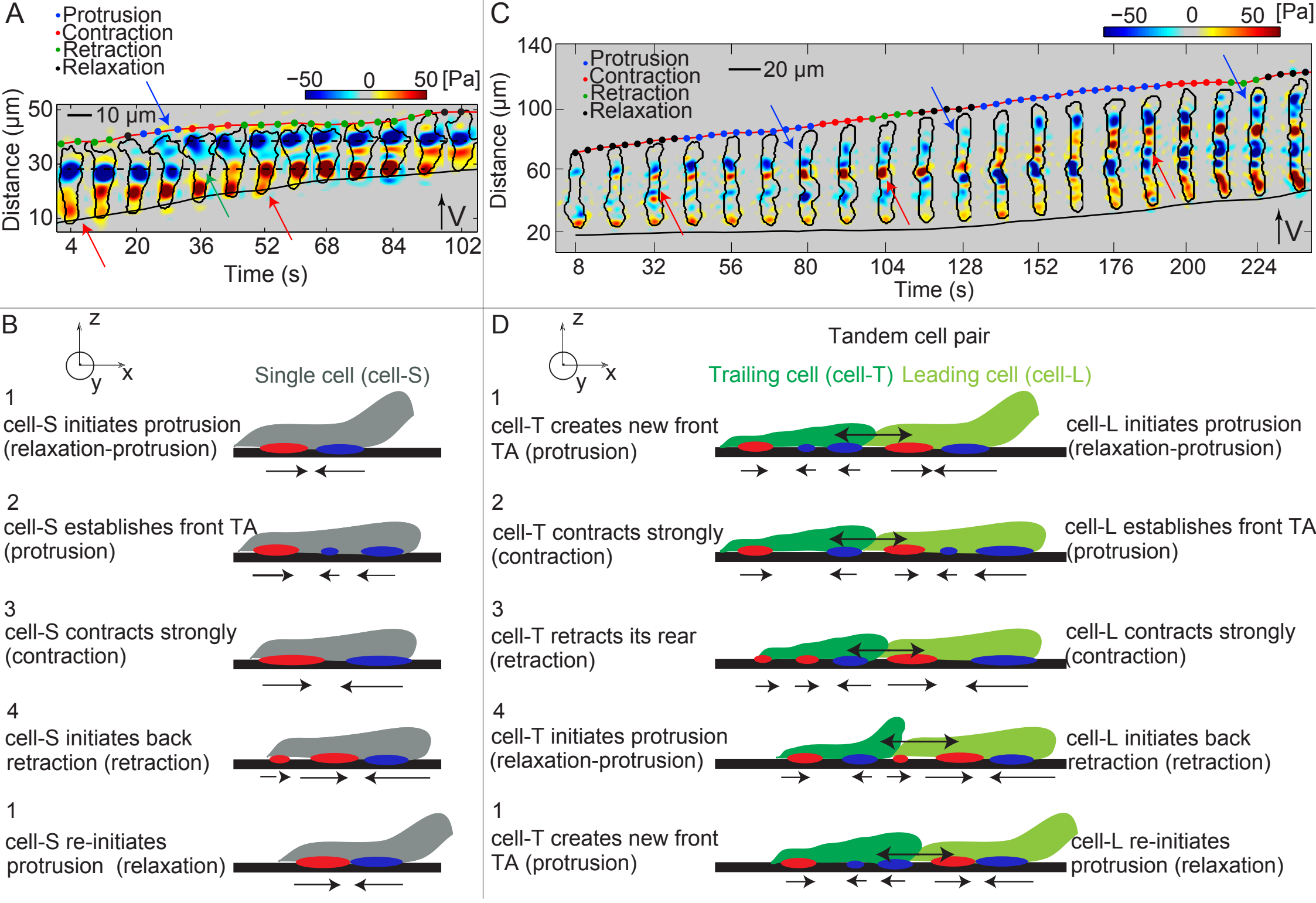

Bastounis et al., Figure S3

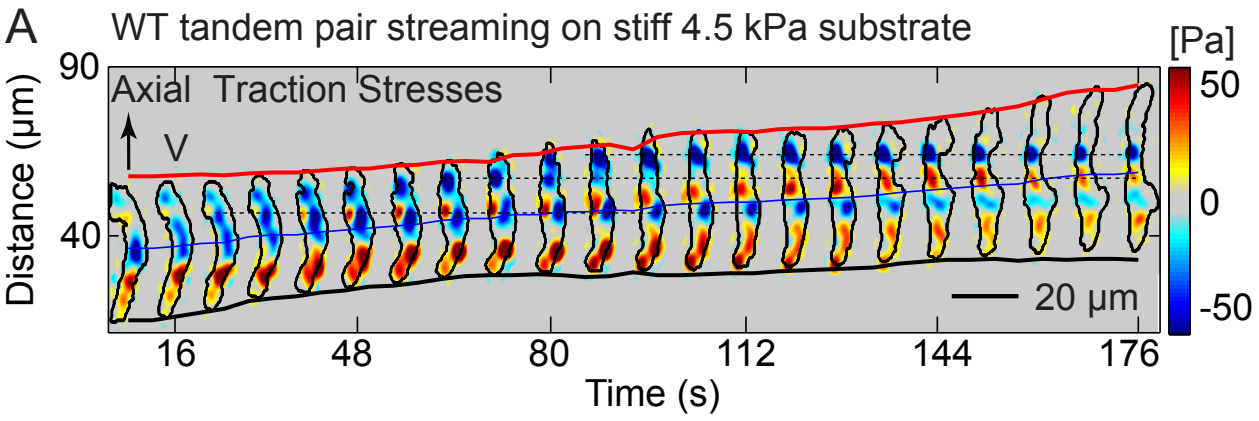

Bastounis et al., Figure S4

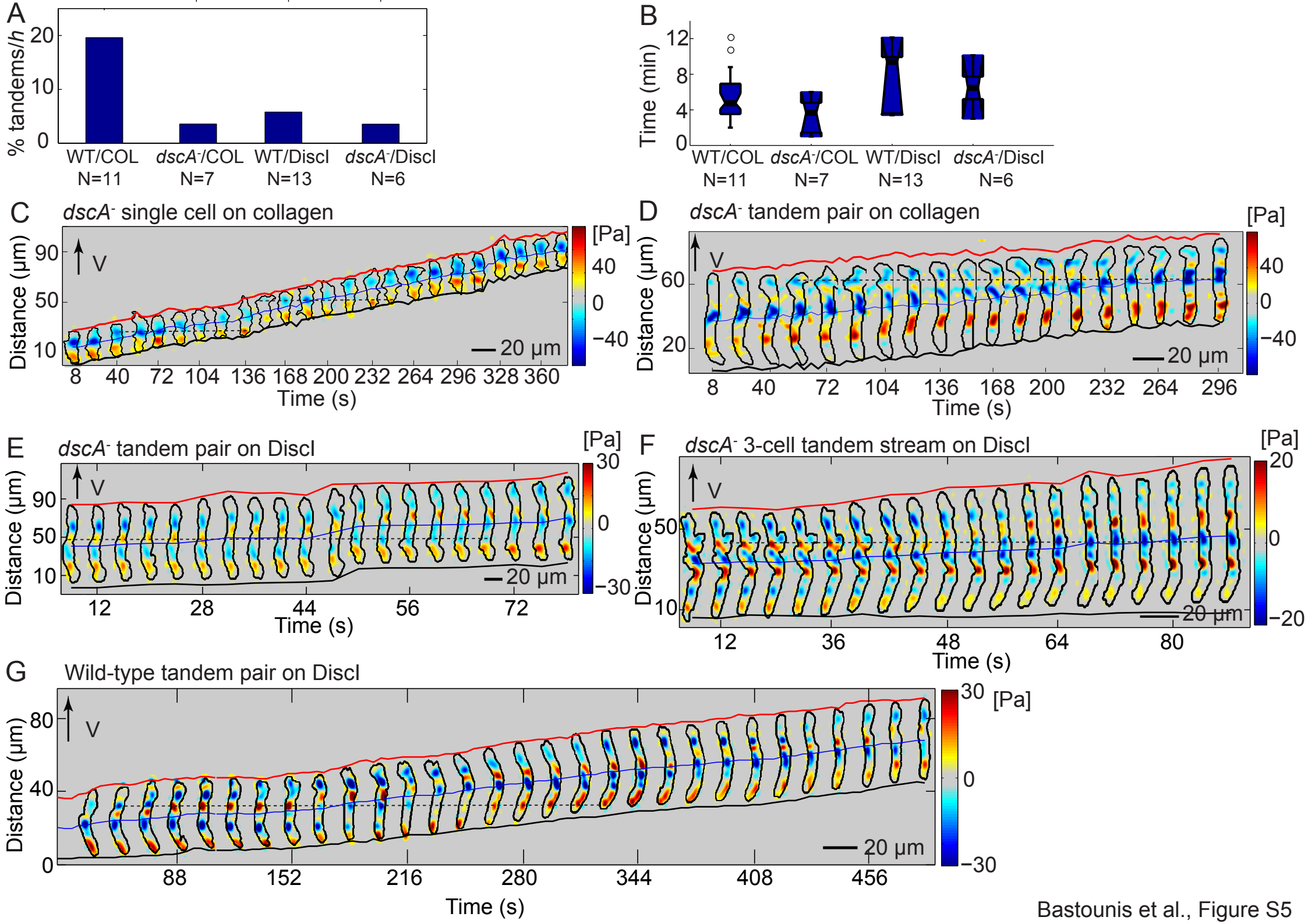

Bastounis et al., Figure S5

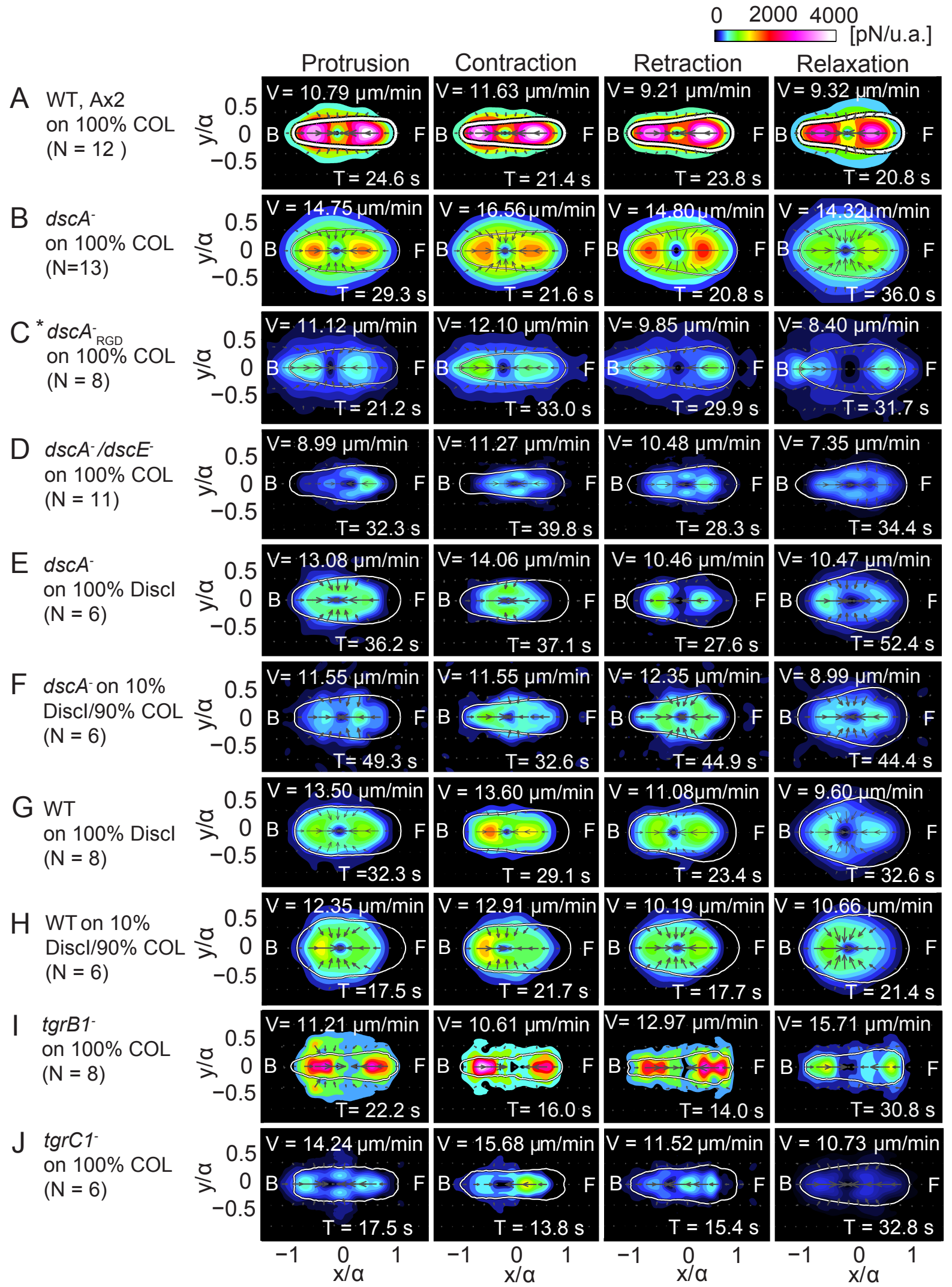

* *dscA*$^{-}_{RGD}$:expressing dscA with RGD deletion

Bastounis et al., Figure S6

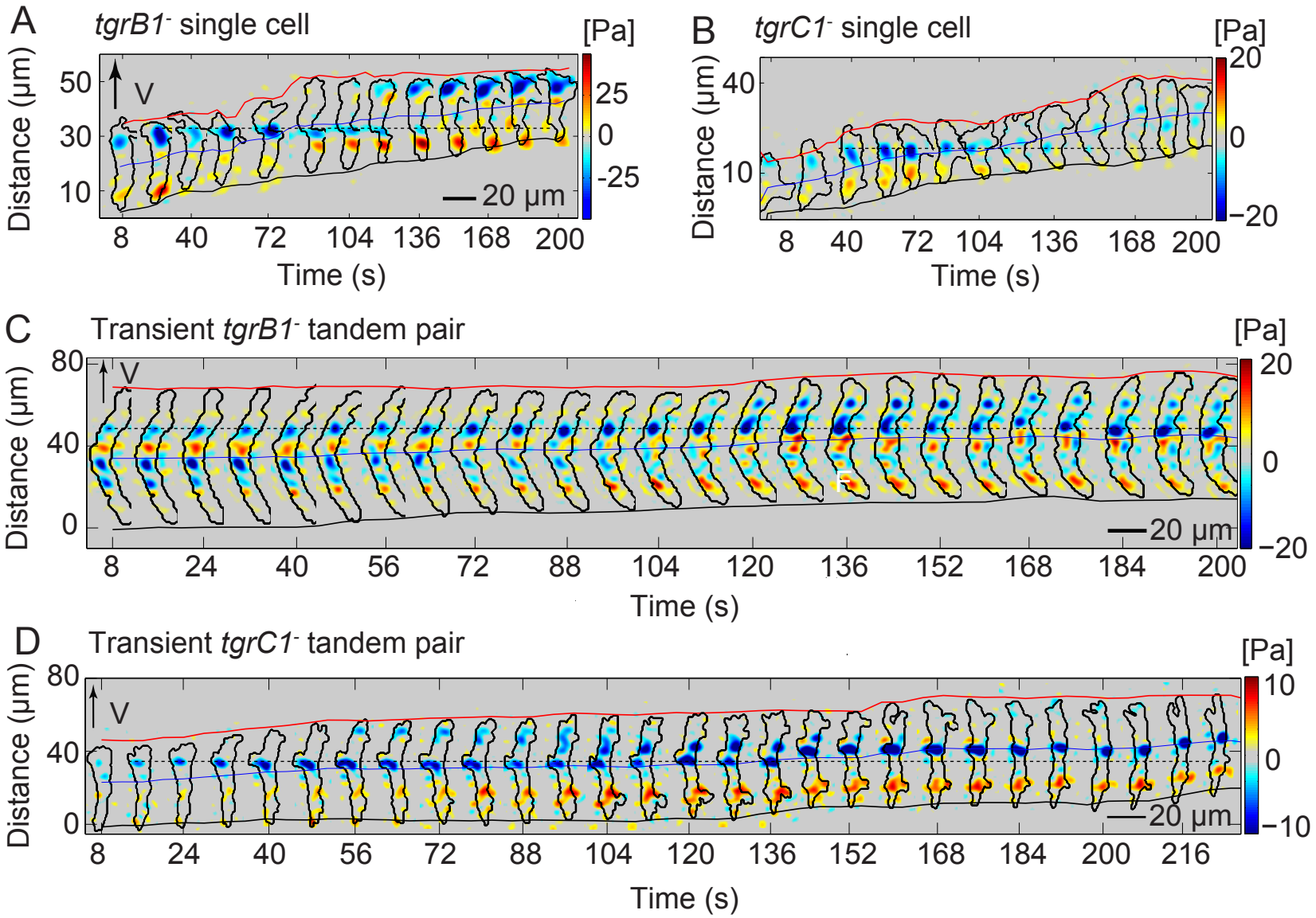

Bastounis et al., Figure S7

SUPPLEMENTAL MATERIALS

SUPPLEMENTAL FIGURE LEGENDS

Figure S1. Tandem wild-type pairs migrate by alternating between 2 motility modes with distinct TA dynamics. (**A**) Spatiotemporal kymographic representation of the instantaneous axial traction stresses as a function of the position along the streaming pair's trajectory, x, and time, t. At any given instant of time, the centroid of the pair is displaced vertically according to its motion, so that the pair is moving from bottom to top. The blue line indicates the pair's centroid, which should coincide roughly with the border between the two cells. The inclined red and black lines indicate the instantaneous position of the front and back pair edges. The black contours are the pair's outlines, shown every 16 s. The dots superimposed on the front edge of the leading cell indicate the phases of the cycle of the leading cell identified by the oscillations of the total elastic energy exerted on the substratum by the pair. The pair alternates between motility Modes 1 and 2, based on whether it acts as one contractile dipole or two. The respective Modes 1 and 2 (M1: red, M2: blue) at each instant of time are indicated and have been identified using K_x (see Supplemental Materials and Methods). **(B)** Representation of K_x using a 3D wireframe mesh plot. Horizontal axes show distance travelled and time while the vertical axis (surface height) shows the magnitude of K_x. Note that for time periods in which the pair is in M2 K_x displays only one local maximum whereas when the pair is employing M1 there are two local maxima displayed (corresponds to Figure 2).

Figure S2. Motility parameters of single chemotaxing wild-type cells and tandem wild-type pairs. (A-C) Boxplots of motility parameters corresponding to single chemotaxing wild-type cells (blue, N = 12) and tandem wild-type pairs (red, N = 14). **(A)** Speed of migration (V). **(B)** Lateral versus axial force (F_y / F_x). **(C)** Total strain energy (U_s). (**D**) Table comparing the average and standard deviation of V (2nd column), U_s (3rd column) and F_y / F_x (fourth column) for single chemotaxing wild-type cells (2nd row), tandem pairs in Mode 1 (M1, third row) and tandem pairs in Mode 2 (M2, fourth row). Circles represent outliers, and the notched section of the boxplots shows the 95% confidence interval around the median (Wilcoxon-Mann-Whitney test). One or two asterisks

denote statistically significant differences between the median of two distributions (<0.05 or <0.01 respectively, Wilcoxon ranksum test) (corresponds to Figure 3).

Figure S3. Protrusion of the leading and trailing cells of a tandem pair do not occur concurrently. (A) Kymograph of the instantaneous axial traction stresses for a representative single chemotaxing cell. The instantaneous axial stresses and cell contours (black) are displayed every 8 s. The dots superimposed on the cell's front edge indicate the phases of the cycle. Blue arrow indicates the instant of time where a new front TA is formed. Red arrows indicate the instants of time where a back TA is lost at the back of the cell. Green arrow shows the instant of time when a front TA gets unloaded and becomes a back TA. **(B)** Schematic representation of the TA dynamics and the motility cycle phases of a single cell (cell-S). Gray contours are representations of the side view of cell-S, while front (blue ovals) and back (red ovals) TAs are shown as ellipses beneath the cell-S. The horizontal black line indicates the side view of the substratum on which the cell-S migrates from left to right. Black arrows show the direction of the contractile axial forces underneath the TAs. **1.** Cell-S initiates protrusion (relaxation phase) while actively adhering at two sites. **2.** Cell-S establishes a new front TA (protrusion phase) while its previous front TA nears the middle of the cell-S and progressively gets unloaded. **3.** Cell-S contracts strongly by adhering at two TAs at its front and back halves (contraction phase). **4.** Cell-S initiates retraction of its trailing edge (retraction phase), its old back TA gets unloaded, while its old front TA becomes the newly formed back TA. **(C)** Same as panel **A** for a representative tandem cell pair. The instantaneous axial stresses and pair contours (black) are displayed every 12 s. The dots superimposed on the leading cell's front edge indicate the phases of the cycle based on the oscillations of the total strain energy. Blue arrows indicate the instants of time when a new front TA is formed at the front half of the leading cell. Red arrows indicate the instants of time when a new front TA is formed at the front half of the trailing cell. **(D)** Schematic representation of the TA dynamics and the motility cycle phases of a streaming tandem cell pair, similar to that presented in panel A (leading cell: light green, cell-L; trailing cell: dark green, cell-T). Since wild-type pairs are most of the time employing motility Mode 1, for simplicity we assume that the pairs are always acting as two contractile dipoles. **1.** Cell-L initiates protrusion (relaxation phase) while cell-T forms its

new front TA (protrusion phase). **2.** Cell-L establishes its new front TA (protrusion phase) while cell-T contracts strongly by actively adhering at two TAs at its front and back halves (contraction phase). **3.** Cell-L contracts strongly by adhering at two TAs (contraction phase) while cell-T retracts its back edge, breaking its old back TA (retraction phase). **4.** Cell-L initiates retraction of its trailing edge (retraction phase) and progressively unloads its back TA, while cell-T initiates front protrusion (protrusion phase) (corresponds to Figure 4).

Figure S4. Tandem wild-type pairs still re-use their TAs when migrating on substrata of increased stiffness. Spatiotemporal kymographic representation of the instantaneous axial traction stresses as a function of the position along a streaming pair's trajectory, x, and time, t. The pair is migrating on a 4.5 kPa collagen-coated gel. At any given instant of time, the centroid of the pair is displaced vertically according to its motion, so that the pair is moving from bottom to top. The blue line indicates the pair's centroid, which should coincide roughly with the border between the two cells. The inclined red and black lines indicate the instantaneous position of the front and back pair edges. The black contours are the pair's outlines, shown every 16 s. The black dotted line shows that the TAs are re-used as the pair migrated forward (corresponds to Figure 6).

Figure S5. **Both migration in dscA-coated substrata and ablation of dscA leads to formation of less tandem pairs. (A)** Percentage of tandem cell pairs formed per hour by wild-type and *dscA*$^-$ cells moving on collagen-coated substrata (COL) and by wild-type cells and *dscA*$^-$ cells moving on DiscI-coated substrata (DiscI). N indicates the number of independent recordings analyzed. **(B)** Time that the pairs remain together once they are formed for wild-type and *dscA*$^-$ cells moving on collagen-coated substrata (COL) and for wild-type cells and *dscA*$^-$ cells moving on DiscI-coated substrata (DiscI). **(C-G)** Spatiotemporal kymographic representation of the instantaneous axial stresses for a representative chemotaxing single *dscA*$^-$ cell migrating on collagen-coated substratum (C), a *dscA*$^-$ tandem pair migrating on collagen-coated substratum (D), a *dscA*$^-$ tandem pair migrating on DiscI-coated substratum (E), a *dscA*$^-$ 3-cell stream migrating on DiscI-coated substratum (F) and a wild-type tandem pair migrating on DiscI-coated substratum (G) (for details see Figure

2B). Blue line shows the cell or cell pair centroid. Black dashed lines follow representative spatially stationary TAs (corresponds to Figure 7).

Figure S6. Phase average stress maps of single chemotaxing wild-type and mutant cells. (A-J) Phase-average traction stress maps in the cell-based reference frame for single chemotaxing cells of different cell lines. Each column shows the magnitude of the total stresses of each different phase of the motility cycle for each cell line (row). For each phase average, the average phase duration (*T*) and speed (*V*) are displayed. B and F indicate the back and the front of the cell respectively. **(A)** Wild-type cells chemotaxing on 100% collagen-coated substrata (N = 12). **(B)** *dscA*$^{-}$ cells chemotaxing on 100% collagen-coated substrata (N = 13). **(C)** *dscA*$^{-}$ cells expressing dscA with the RGD amino acids deleted chemotaxing on 100% collagen-coated substrata (N = 8). Notice that these mutants exert even lower stresses than *dscA*$^{-}$ cells, suggesting that: (1) the RGD sequence is important for the ability of the DiscI lectin to be functional; (2) or that the RGD sequence of the lectin plays a role in cell-substratum adhesion; (3) or that there is a dominant negative phenotype since cells also express dscE. **(D)** *dscA*$^{-}$ and *dscE*$^{-}$ double knock-out cells chemotaxing on 100% collagen-coated substrata (N = 11). **(E)** *dscA*$^{-}$ cells chemotaxing on 100% DiscI-coated substrata (N = 6). **(F)** *dscA*$^{-}$ cells chemotaxing on 10% DiscI and 90% collagen coated substrata (N = 6). **(G)** Wild-type cells chemotaxing on 100% DiscI-coated substrata (N = 8). **(H)** Wild-type cells chemotaxing on 10% DiscI and 90% collagen coated substrata (N = 6). **(I)** *tgrB1*$^{-}$ cells chemotaxing on 100% collagen-coated substrata (N = 8). **(J)** *tgrC1*$^{-}$ cells chemotaxing on 100% collagen-coated substrata (N = 6) (corresponds to Figure 7).

Figure S7. ***tgrB1***$^{-}$ **and** ***tgrC1***$^{-}$ **transiently formed pairs still re-use their TAs. (A-D)** Spatiotemporal kymographic representation of the instantaneous axial stresses for a representative a representative chemotaxing single *tgrB1*$^{-}$ cell (A), a single *tgrC1*$^{-}$ cell (B), a transient tandem *tgrB1*$^{-}$ pair (C) and a transient tandem *tgrC1*$^{-}$ pair (D). Blue line shows the cell or cell pair centroid. Black dashed lines follow representative spatially stationary TAs (corresponds to Figure 7).

SUPPLEMENTAL VIDEO LEGENDS

Video 1. **DIC time-lapse movie and traction stresses exerted by a tandem wild-type *Dictyostelium* pair moving on a collagen-coated polyacrylamide substratum.** The contour of the pair is shown in black. The magnitude of the traction stresses that the pair exerts is indicated with the blue colormap shown on the upper right part of the movie [Pa]. The scale bar is 10 μ m long. Time-lapse sequences were acquired every 4 s on a Nikon TE300 inverted light microscope controlled by the MetaMorph software (Molecular Devices, Sunnyvale, CA). Calculation of the traction stresses and generation of the video images were performed using MATLAB (Mathworks Inc, Natick, MA). The video refers to the tandem pair shown in Figure 2 but includes additional time points. Playback rate is 40× real time (10 frames/s) (corresponds to Figure 1).

Video 2. **Time evolution of the axial traction stresses and corresponding progressive emergence of the axial tension kymograph for a streaming tandem wild-type *Dictyostelium* pair.** The tension kymograph of a representative tandem pair, shown on the left, is progressively built by adding the traction tension T_x at each instant of time while the instantaneous pair contour (black) moves upward with the pair's centroid velocity V. Red and black lines indicate the position of the front and back pair edge. Motility has been split into cycles comprised by four phases, based on the quasi-periodic oscillations of the total strain energy of the pair and by using phase statistics. All individual time points have been assigned to the four phases and are shown as colored dots superimposed on the red line showing the front cell edge (blue, protrusion; red, contraction; green, retraction; black, relaxation). The insert in the upper left corner shows the oscillations of the strain energy, $U_s(t)$ (blue line) and the current value of $U_s(t)$ (red circle). The graph on the right shows the instantaneous axial traction stresses together with the instantaneous outline of the pair (black contour). Time-lapse sequences were acquired every 4 s on a Nikon TE300 inverted light microscope controlled by the MetaMorph software (Molecular Devices, Sunnyvale, CA). Calculation of the traction stresses and tension and generation of the video images were performed using MATLAB (Mathworks Inc, Natick, MA). The video refers to the tandem cell pair shown in Figure 2 but includes additional time points. Playback rate is 40× real time (10 frames/s) (corresponds to Figure 2).

Video 3. **3D shape changes, F-actin localization and traction stresses of a tandem wild-type pair implementing only Mode 1**. Cells were transformed to generate lines expressing *Lifeact* (Abp140-GFP) to define the pair's 3D shape. Z-stacks of each time-lapse sequence of the pair were acquired every 12 s on a spinning disk confocal microscope (Leica DMIRE2, Yokogawa CSU10) controlled by Slidebook software (3I, Denver). Calculation of the traction stresses was performed using MATLAB. The 3D pair's shape is shown in gray and the rendering of the shape as well as the generation of this video was performed using the IMARIS software (Bitplane, Zürich, Switzerland)). The panel on the left side shows the 3D pair shape together with the traction stresses it exerts on its substratum. The panel on the right side shows the 3D pair's shape together with the localization of F-actin. The pair moves from left to right. Note that the pair always actively adheres at 4 TAs, suggesting that it only implements Mode 1, moving as two contractile dipoles. The movie corresponds to Figure 3 and is accelerated 24× real time (corresponds to Figure 3).

Video 4. **3D shape changes, F-actin localization and traction stresses of a tandem wild-type *Dictyostelium* pair implementing Modes 1 and 2**. Same as Video 3 but for a tandem pair implementing Mode 2 (3 TAs, frames 1-5) and then Mode 1 (4 TAs, frames 6-19) and moving from left to right. The movie corresponds to Figure 3 and is accelerated 24× real time (corresponds to Figure 3).

Video 5. **DIC time-lapse movie of wild-type *Dictyostelium* cells moving on a collagen I-coated polyacrylamide substratum.** Cells were pulsed for 8 h and time-lapse DIC sequences were acquired every 4 s on a Nikon TE300 inverted light microscope controlled by the MetaMorph software (Molecular Devices, Sunnyvale, CA). Playback rate is 40× real time (10 frames/s) and scale bar is 10 μm long (corresponds to Figure 7).

Video 6. **DIC time-lapse movie of wild-type *Dictyostelium* cells moving on a DiscI-coated polyacrylamide substratum.** Cells were pulsed for 8 h and time-lapse DIC sequences were acquired every 4 s on a Nikon TE300 inverted light microscope controlled by the MetaMorph software (Molecular Devices, Sunnyvale, CA). Playback rate is 40× real time (10 frames/s) and scale bar is 10 μm long (corresponds to Figure 7).

Video 7. **DIC time-lapse movie and traction stresses exerted by a tandem wild-type *Dictyostelium* pair moving on a DisclI-coated polyacrylamide substratum.** The contour of the pair is shown in black. The magnitude of the traction stresses that the pair exerts is indicated with the colormap shown on the upper right part of the movie [Pa]. The scale bar is 10 μm long. Time-lapse sequences were acquired every 4 s on a Nikon TE300 inverted light microscope controlled by the MetaMorph software (Molecular Devices, Sunnyvale, CA). Calculation of the traction stresses and generation of the video images were performed using MATLAB (Mathworks Inc, Natick, MA). Playback rate is 40× real time (10 frames/s) (corresponds to Figure 7).

Video 8. **DIC time-lapse movie and traction stresses exerted by a tandem wild-type *Dictyostelium* pair performing a turn while moving on a collagen-coated polyacrylamide substratum.** The contour of the pair is shown in black. The magnitude of the traction stresses that the pair exerts is indicated with the colormap shown on the upper right part of the movie [Pa]. The scale bar is 10 μm long. Time-lapse sequences were acquired every 4 s on a Nikon TE300 inverted light microscope controlled by the MetaMorph software (Molecular Devices, Sunnyvale, CA). Calculation of the traction stresses and generation of the video images were performed using MATLAB (Mathworks Inc, Natick, MA). Playback rate is 40× real time (10 frames/s) (corresponds to Figure 7).

Video 9. **DIC time-lapse movie of *tgrB1*$^-$ cells moving on a collagen-coated polyacrylamide substratum.** Cells were pulsed for 8 h and time-lapse DIC sequences were acquired every 4 s on a Nikon TE300 inverted light microscope controlled by the MetaMorph software (Molecular Devices, Sunnyvale, CA). Playback rate is 40× real time (10 frames/s) and scale bar is 10 μm long (corresponds to Figure 7).

Video 10. **DIC time-lapse movie of *tgrC1*$^-$ cells moving on a collagen-coated polyacrylamide substratum.** Cells were pulsed for 8 h and time-lapse DIC sequences were acquired every 4 s on a Nikon TE300 inverted light microscope controlled by the MetaMorph software (Molecular Devices, Sunnyvale, CA). Playback rate is 40× real time (10 frames/s) and scale bar is 10 μm long (corresponds to Figure 7).

SUPPLEMENTAL MATERIALS AND METHODS

Dictyostelium culture and microscopy

Dictyostelium cells were grown under axenic conditions in HL5 growth medium on tissue culture plates. We used the following cell lines: wild-type cells (Ax2, obtained from the *Dictyostelium* Stock Center), *dscA*$^-$ cells (generated from Ax2, in our laboratory), *dscA*$^-$/*dscE*$^-$ double knock-out cells (generated from Ax2, in our laboratory). We also used wild-type cells Ax4, *tgrC1*$^-$.and *tgrB1*$^-$ cells, a generous gift from Prof G. Shaulsky (Baylor College of Medicine). We transformed all cell lines to generate lines expressing *Lifeact* (Abp140-GFP) (Riedl *et al.*, 2008), a 17 amino-acid peptide which binds F-actin. We prepared aggregation-competent cells as described elsewhere (Meili *et al.*, 1999). For all chemotaxis applications, cells were taken from axenic exponentially growing or "log-phase" cultures, by shaking cells in nutrient medium, in an autoclaved Erlenmeyer flask at 150 rpm, 22^{o}C, overnight. The next morning cells were counted using a hematocytometer to determine cell density. Aggregation competent cells were prepared by pulsing a 5 x 10^6 cells/ml suspension in Na/K phosphate starvation buffer (9.6 mM KH_2PO_4, 2.4 mM Na_2HPO_4, pH 6.3) with cAMP to a concentration of 30 nM every 6 min for 6 h (Meili *et al.*, 1999) for single cell chemotaxis and for 8 h for cell pair streaming. For chemotaxis of single cells and cell pair streaming, cells were diluted in Na/K phosphate buffer at low density (1 x 10^5 cells/ml and 4 x 10^5 cells/ml respectively) and 200 μl of cells were seeded onto a flat elastic collagen-coated polyacrylamide substratum and allowed to adhere. A drawn glass capillary mounted on a micromanipulator served as the source of chemoattractant (150 mM cAMP in an Eppendorf femtotip, Eppendorf, Germany).

We acquired images using a Nikon TE300 inverted microscope with a Plan Fluor 40X 0.6 NA air objective and a cooled CCD camera (HQ CoolSnap, Roper Scientific). A PC running Metamorph software (Molecular Devices, Downington, PA) controlled the entire setup including filter wheels. For the image acquisition of the cells expressing the *Lifeact* marker, we used a spinning disk confocal microscope (Leica DMIRE2, Yokogawa CSU10) with a Plan Apo 40X 1.4 NA oil objective w and a PC running Slidebook software (3I, Denver) to control the entire setup. The microscope was equipped with an ASI piezo-Z actuator.

Construction of the *dscA*$^-$ single knock-out cell line

To construct the *dscA*$^-$ null strain, the dscA gene was amplified split in two parts. Part1 (PCR1) was amplified from gDNA using the forward primer GTTACTAGTAAAGTAGTTTAACTTCATAGTG and the reverse primer GTTGGATCCCCCAGGTTAATGGGTGGATAGC. Similarly, part 2 (PCR2) was amplified from gDNA using the forward primer GTTGGATCCGCTATCCACCCATTAACCTGG and the reverse primer GTTAAGCTTCTCTTCCAAGCTAAGTAAGCCTTAC. PCR1 was purified and digested with *Spe*I and *Bam*HI restriction endonucleases. PCR2 was purified and digested with *HINDIII* and *Bam*HI restriction endonucleases. PCR1 and PCR2 were ligated to the SK (pBluescript) vector. The Bsr cassette was then inserted to the *Bam*HI site. We also performed sequencing to the dscA domain to ensure mutation free DNA. The DNA was then electroporated into wild-type AX2 cells selecting for Bsr-resistant clones after 5 d in Bsr-containing medium. To assess complementation, a 3' GFP construct was inserted to dscA and expressed in *dscA*$^-$ cells.

Construction of the *dscE*$^-$ and *dscA*$^-$/*dscE*$^-$ double knock out cell line

To construct the *dscE*$^-$ null strain, dscE gene was amplified split in two parts. Part1 (PCR1) was amplified from gDNA using the forward primer GTTACTAGTTTAAAAAACAGACAGTCAAAACACAGCACC (300bp upstream of ATG) and the reverse primer GTTAGATCTAATATGATTATTATAGGTTTGAGGATGAATGGC. Similarly, part 2 (PCR2) was amplified from gDNA using the forward primer GTTAGATCTTTTATGCATTACCAGTTAAAAGTTATTC and the reverse primer GTTCTCGAGTGAAGAGTAGTTATATGATAATTGATTC (300bp downstream of stop codon). PCR1 was purified and digested with the *Spe*I and *BglII* restriction endonucleases. PCR2 was purified and digested with the *XhoI* and *BglII* restriction endonucleases. PCR1 and PCR2 were ligated to the SK (pBluescript) vector. Bsr or hygro cassette then was inserted to the *Bgl*II site. We also performed sequencing to the dscE domain to ensure mutation free DNA. The DNA was then electroporated into wild-type AX2 cells selecting for Bsr or *dscA*$^-$ cells selecting for hygro-resistant cells.

Polyacrylamide gel fabrication and characterization

12 mm diameter and approximately 40 μm thick polyacrylamide hydrogels were prepared using 5% acrylamide and 0.06% bis-acrylamide (Young's modulus ~1200 Pa) on a glass carrier and were coated with 0.25 mg/ml collagen I and used as substrata for our cells (Wang and Pelham, 1998; Engler *et al.*, 2004). The gels consist of two layers: the bottom layer contains no beads; and the upper one contains 0.04% (by volume) carboxylate-modified red latex beads of 0.1 μm diameter (FluoSpheres; Molecular Probes, Eugene, OR). To improve the signal to noise ratio, the polyacrylamide gel was fabricated as two sequential layers with the first bottom one containing no beads and the second top one containing 0.03% carboxylate modified yellow latex beads with 0.1 μm diameter (Fluospheres, Molecular Probes, Eugene, Oregon). The exact protocol we followed consisted of three steps described below:

1. Lower glass coverslip treatment: 25 mm glass coverslips were placed on a hot plate and 500 μL of 0.1 M NaOH were added to cover the entire surface of the coverslips. Once the liquid evaporated, leaving a uniform, white thin film of NaOH on the surface, the coverslips were removed from the plate and placed in a fume hood. The coverslips were covered with 100μL of 3-Aminopropyltriethoxysilane (APTS) for 5 min and then rinsed thoroughly with distilled water. The coverslips were dried and 100μL of a premixed solution of 0.5% glutaraldehyde in PBS buffer was added to them and was let stand for 30 min. The coverslips were then rinsed and dried and ready for gel attachment.

2. Preparation of the two gel layers: The polyacrylamide gel consisted of two layers, the bottom one containing no beads and the upper one containing 4 μL of 2% carboxylate modified yellow latex beads. Two solutions of 5% acrylamide and 0.06% bis-acrylamide were prepared using 12mM Na/K phosphate starvation buffer (pH 6.3) as solvent and one contained 0.03% carboxylate modified red latex beads (Fluospheres, Molecular Probes, Eugene, Oregon). The solutions were placed on ice in vacuum for 15 min to reduce dissolved oxygen. 0.8 μL of TEMED (crosslinker) and 1.2 μL of 10% APS (catalyst) were added to the solution containing no beads and then 3.6 μL of the mixture was placed at the center of circular glass coverslips which were positioned on top of the treated square coverslips to "sandwich" the polyacrylamide gel. When the gel polymerized (10-30 min), the

second layer containing the tracker beads was added in a similar manner and some weight was placed on the top coverslip to make the bead-containing layer slightly thinner. The square coverslips with the two layers on top of them were then mounted into Petri dishes filled with 50 mM HEPES buffer (pH 8.5) using silicon grease (Dow Corning, Midland, Michigan).

3. Inspection of the gel and activation with Sulfo-SANPAH: Gels were examined under the microscope to verify that the distribution of beads was uniform and the layer of beads was confined in one focal plane (the uppermost) or otherwise discarded. We then crosslinked collagen I (or any other protein of interest) to the surface of the gels using 200 µl of 0.5 mg/ml Sulfo-SANPAH (Thermo Sci, Rockford, Il) in 50 mM HEPES buffer pH 8.5. After 10 min of UV activation and washing thoroughly, 200 µl of 0.25 mg/ml collagen I protein in 50 mM HEPES buffer pH 8.5 was added and the gels were incubated overnight at room temperature. After washing, the gels were stored with buffer (50mM HEPES buffer, pH 8.5) and antibiotic (40 mM Ampicillin) for use within a week. Substratum thickness was measured by locating the top and bottom planes of the gel and subtracting their z positions. The gels were stored in 4^{o}C and could be used within one week.

4. Mechanical characterization of the gel: We measured the (Keer, 1964) substratum thickness by locating the top and bottom planes of the gel and subtracting their z positions. The Young modulus (~1200 Pa) was verified from measurements of the indentation of a tungsten carbide sphere (Keer, 1964) and also using atomic force microscopy.

Discoidin I Purification

A plasmid for the expression of discoidin I (DiscI) was generously provided by Prof. A. Varrot (CERMAV-CNRS, Université Joseph Fourier and Institut de Chimie Moléculaire de Grenoble). dscA was purified as described (Mathieu et al., 2010) with modifications. The protein was overexpressed in *E.coli* Rosetta2(DE3)plysS bacterial competent cells and Luria broth medium. Cells were cultured at 37 °C in an orbital shaker, up to an optical density of ~1.2 at 600 nm before overnight induction with 0.2 mM IPTG at 16 °C. Cells were harvested by centrifugation at 5,000 g and each gram of cells was resuspended in 25 ml of buffer A [20 mM Tris–HCl (pH 8.5), 3\00 mM NaCl, and 10 mM imidazole] before using a Microfluidizer for

cell disruption. Cells were lysed by two Microfluidizer (Microfluidics) cycles at 80,000 psi. The lysed cells were centrifuged at 60,000 g for 30 min and the supernatant was collected and loaded onto a 5-ml Histrap™ column (GE Healthcare). After a wash step of 5 -10 column volumes with buffer A, dscA was eluted with a 10–500 mM imidazole gradient. Imidazole was removed using a PD10 column (GE Healthcare) equilibrated with 20 mM Tris–HCl (pH 7.5) and 150 mM NaCl. The pure protein was concentrated to ~2 mg /ml using a YM10 Amicon centrifugation device.

Single cell and cell pair identification

We acquired differential interference contrast (DIC) images using a 40 X air lens at 4 s intervals for both studying single *Dictyostelium* cells and streaming tandem pairs. Time-lapse fluorescent confocal images were acquired using a 40 X oil immersion lens at 12 s intervals. For each time point, *z*-stacks along the cell or cell pair height were also acquired with a *z*-spacing of 1 μm (typically 15 images). We used a MATLAB (Mathworks Inc, Natick, MA) custom algorithm to automatically identify the contour of the cells (or tandem pairs) from the DIC images and the fluorescent confocal images (del Álamo *et al.*, 2007). Briefly, in the case of the DIC images, imperfections were removed from the individual images using the average of the image series. A threshold was then applied to the resulting images to extract the most intense features, which were refined using two consecutive image dilations and erosions with structuring elements of increasing size. Details of the exact contour identification method can be found elsewhere (del Álamo *et al.*, 2007). For the fluorescent confocal images, the contour of the cell (or tandem pair) was found by setting a predefined, constant threshold. In the case of the fluorescent confocal images, we performed the 3D reconstruction (rendering) of the cell (or tandem pair) using IMARIS software (Bitplane, Zürich, Switzerland).

The location of the centroid (center of mass) (x_c, y_c), and the orientation of the major and minor moments of inertia (longitudinal and transverse axes) of each cell (or tandem pair) were calculated using standard MATLAB functions. We determined the front and back halves of the cell (or tandem pair) as the two

parts in which the minor axis of inertia splits each cell (or tandem pair), with the front pointing towards the direction of motion (del Álamo *et al.*, 2007).

Measurements of the substratum deformation

As the cells apply traction forces, they induce deformations on the elastic substratum on which they attach. We measured the deformation of the substratum from the displacements of the fiduciary fluorescent beads embedded in the upper layer of the substratum. Briefly, at each time interval, we measured the 2D deformation of the substratum at each point using a technique similar to Particle Image Velocimetry (Willert and Gharib, 1991; Gui and Wereley, 2002). We calculated the local deformation vector by performing an image correlation between each image and the unstretched reference image. We used interrogation windows of 16 x 16 pixels with a 50% overlap. Further details of this technique can be found elsewhere (del Álamo *et al.*, 2007).

Calculation of the traction stresses, strain energy, construction of the axial tension kymograph and classification in streaming motility modes

The traction stress field (traction force per unit area) exerted by the cells (or tandem pairs) on the surface of the substratum was calculated from the measured deformation using in-house Fourier Traction Force Microscopy (FTFM) methods (del Álamo *et al.*, 2007) that can be downloaded at http://maeresearch.ucsd.edu/~jalamo/dynacyte. These methods consist of solving analytically the elastostatic equation of equilibrium for a linear, homogeneous, isotropic, 3D body using Fourier series and taking into account the finite thickness of the substratum (h), thus improving the accuracy of previous methods based on unconstrained FTFM (Butler *et al.*, 2002). The thickness of the substratum h was on average 40 μm, the measured Young's modulus E of the substratum was 1.2 kPa (Bastounis *et al.*, 2011), and the Poisson's ratio σ was assumed ~ 0.45, as reported in previous studies (Li *et al.*, 1993; Engler *et al.*, 2004; Frey *et al.*, 2007).
The boundary conditions used were: no slip at the base of the substratum ($\vec{u}(x,y,0) = 0$, where $\vec{u} = u\vec{\imath} + v\vec{\jmath}$); the displacements at h_0 ($u(x,y,h_0) = u^{h_0}(x,y)$ and $v(x,y,h_0) = v^{h_0}(x,y)$); and the vertical stress $\tau_{zz}(z =$

$h) = 0$, since the density of the cells and the surrounding buffer are similar and the contractile fibers of the cytoskeleton tend to predominantly orient horizontally. We assumed periodicity in the horizontal directions. Therefore the equations governing the displacement field for a linear, homogeneous, isotropic, 3D body of finite thickness are:

$$\frac{\nabla(\nabla\cdot\vec{u})}{(1-2\sigma)} + \Delta\vec{u} = 0 \text{ (1)}$$

We find the solution of the elastostatic equation using Fourier series:

$$\bar{\tau}(x,y,z) = \sum_{\alpha=1}^{\infty}\sum_{\beta=1}^{\infty}\hat{\bar{\tau}}_{\alpha\beta}(z)e^{2\pi i\alpha x}e^{2\pi i\beta y} \text{ (2) and } \vec{u}(x,y,z) = \sum_{\alpha=1}^{\infty}\sum_{\beta=1}^{\infty}\hat{\vec{u}}_{\alpha\beta}(z)e^{2\pi i\alpha x}e^{2\pi i\beta y} \text{ (3)}$$

where α, β are the wavenumbers for the x, y directions and $\hat{\bar{\tau}}_{\alpha\beta}(z)$, $\hat{\vec{u}}_{\alpha\beta}(z)$ are the complex Fourier coefficients for $\bar{\tau}$, $\vec{u}$, which are functions of the vertical coordinate and are linearly related to the Fourier coefficients of the horizontal displacements measured at $z = h_0$. A mathematical derivation of the solution is provided in (del Álamo *et al.*, 2007).

Once the cell (or tandem pair) contour was determined from the differential interference contrast (DIC) images, we identified the location of the major and minor second moments of inertia and the orientation of their axes. The traction stress field $\vec{\tau}(x,y) = \tau_x\vec{\imath} + \tau_y\vec{\jmath}$ was then calculated and rotated to make the cell's (or tandem pair's) major axis parallel to the vertical direction at each instant of time, as illustrated in Figures 1A-3 and B-3, which show the magnitude of the instantaneous traction stresses, $|\vec{\tau}|(x,y)$ for a single cell and a tandem pair respectively. In this new coordinate system, we calculated at each instant of time the axial traction tension by integrating the x-component of the traction stresses across the cell (or tandem pair) width (minor axis, y-direction), as shown in Figures 1 A-5 and B-5 respectively:

$$T_x(x,t) = \int_{y1}^{y2}\tau_x(x,y,t)dy \text{ (4)}$$

The axial traction tension $T_x(x,t)$ defined this way has the dimension of force per unit length and typically is of the order of nN/μm. The tension kymograph was then constructed by stacking different temporal measurements and plotting $T_x(x,t)$ in two dimensions with t in the horizontal axis and the position in the vertical axis (Figure 2C). This representation allows for a detailed quantitative analysis of the coupled evolution of shape changes

and the location and magnitude of the traction forces during single cell and tandem streaming pair migration with high temporal resolution.

We observed that the two cells of the tandem pair contract strongly axially forming 3 or 4 TAs. When 4 TAs are established the TA dynamics of the two cells is the superposition of the TA dynamics of two single cells in series. That is, each cell attaches actively at two sites at its front and back and contracts inwards and therefore the pair acts as two contractile dipoles (Mode 1; Figure 1B). On the contrary, when 3 TAs are established the pair acts as one contractile dipole. The leading cell typically establishes 2 TAs, while the trailing cell is being dragged forward by establishing only 1 TA at its back half. The stresses at the front of the leading cell point toward the back of the cell pair and the rest of the stresses pointing towards the front of the pair (Mode 2; Figure 1C). To be able to distinguish between the instants of time where a cell pair is moving utilizing Mode 1 or Mode 2, we calculated the cumulative integral of the axial traction tension, $T_x(x,t)$ along the length of the cell pair, $K_x(x,t)$ as described below:

$$K_x(x,t) = \int_0^x T_x(x,t)dx \quad (5)$$

where 0 refers to the back cell edge of the trailing cell of the cell pair and $0 \leq x \leq 2L$ with $2L$ being the length of the cell pair and L the approximate length of each cell. When the two cells of the tandem pair are in Mode 1 (2 contractile dipoles), the instantaneous K_x has two local maxima. On the contrary, when the two cells of the pair are in Mode 2 (1 contractile dipole), the instantaneous K_x shows only one maximum. Therefore, we used the number of maxima of K_x as a criterion to split tandem pair migration in two distinct motility modes based on whether the pair acts as one or two contractile dipoles.

We calculated at each instant of time the total strain energy (U_s) as the mechanical work per unit area done by the pair to deform its substratum:

$$U_s = \frac{1}{2}\int_S \vec{\tau}(z=h)\cdot\vec{u}(z=h)dS \quad (6)$$

where $\vec{u}$ is the measured displacement vector field on the free surface of the substratum and $\int_S ()dS$ represents a surface integral. Further details of the calculation of the traction stresses were provided previously (del Álamo *et al.*, 2007; Alonso-Latorre, 2010). Similarly, we calculated at each instant of time the strain energy exerted by

the leading and trailing cells (U_s–L and U_s-T) as the mechanical work per unit area done by the front and back halves of the tandem pair respectively to deform the substratum.

To investigate how directed contractility contributes to cell motility, we decomposed the traction force vector exerted by each cell (or tandem pair) to the substratum into its axial and lateral components F_x and F_y. We then define the axial and lateral contractility F_x and F_y as:

$$F_x = \frac{|F_f|+|F_b|}{2}, \text{ and } F_y = \frac{|F_l|+|F_r|}{2}, \quad (7)$$

where F_f and F_b are respectively the surface integrals of the axial traction stresses exerted by the cell (or tandem pair) in its front and back halves, while F_l and F_r are the surface integrals of the lateral traction stresses that the cell (or tandem pair) exerts at its right and left halves (relative to the cell's or cell pair's major axis):

$$F_f = \iint_{x>0} \tau_x(x,y)dxdy \text{ and } F_b = \iint_{x<0} \tau_x(x,y)dxdy \quad (8)$$

$$F_l = \iint_{y>0} \tau_y(x,y)dxdy \text{ and } F_r = \iint_{y<0} \tau_y(x,y)dxdy \quad (9)$$

Note that F_f = -F_b and F_l = -F_r as the inertia of the cell (or cell pair) is negligible and both the cell and the tandem pair are always in static equilibrium.

Calculation of the cell pair imbalance (error), cell-cell tension and degree of coupling

The integral over the area of the traction stresses that a cell or a tandem pair exert is expected to be equal to zero. The minor imbalances measured are due to experimental measurement error and can be calculated as follows:

$$Error = \left|\iint_{Area} \tau_x(x,y)dxdy\right| / \iint_{Area} |\tau_x(x,y)|dxdy \quad (10)$$

The error tends to be higher for the pairs since the density of cells surrounding them is higher than in single cell experiments. Therefore, cell pairs analyzed with an imbalance higher than 10% were discarded. Similar to Maruthamuthu et al., we considered that the sum of all stresses exerted under the leading cell (cell-L) of the pair alone yields the cell-cell force (T_L) exerted by the leading cell to the trailing cell (Maruthamuthu *et al.*, 2011). Likewise, the sum of all stresses exerted under the trailing cell (cell-T) of the pair alone yields the cell-cell force

(T_T) exerted by the trailing cell to the leading cell. Since the pair needs to be in equilibrium the sum of all stresses exerted by the pair needs to be equal to 0, which implies that $F_{cell-L} = -F_{cell-T}$ as the inertia of the pair is negligible and the pair is in static equilibrium. Therefore:

$$F_{cell-L} = \iint_0^L \tau_x(x,y)dxdy \text{ and } F_{cell-T} = \iint_L^{2L} \tau_x(x,y)dxdy \quad (11)$$

$$\text{and } F_{cell-L} = T_T, F_{cell-T} = T_L \text{ and } T_L = -T_T \quad (12)$$

We define the cell-cell force (intercellular force) as:

$$T = (F_{cell-T} - F_{cell-L})/2 \quad (13)$$

Cells of a tandem pair of a specific cell line may exert higher stresses on the substratum than cells of another cell line and therefore exert increased intercellular force just because they are stronger. To take into account that, we defined another variable to characterize the degree of intercellular force between cells of a pair relative to how strongly these cells actively attach to the substratum. We named this variable, Degree of Coupling (*DOC*) and defined it as:

$$DOC = \frac{2T}{(\iint|\tau_x(x,y)|dxdy)} \quad (14)$$

When two cells of a tandem pair are completely uncoupled, $T = 0$, $F_{cellF} = -F_{cellB} = 0$ and $DOC = 0$. On the other extreme, the maximum amount of coupling between cells occurs when the tandem pair acts as a single contractile dipole, with the leading cell exerting only negative stresses (pointing backwards toward the pair's centroid) and the trailing cell exerting only positive stresses (pointing forward toward the pair's centroid). In the latter case, $F_{cell-L} = -F_{cell-T} = F$, $T = F$, $\iint|\tau_x(x,y)|dxdy = 2F$ and therefore $DOC = 1$.

Cell-based and pair-based reference system, average traction stress maps, and phase average splitting

The shape and the orientation of the cells (or tandem pairs) constantly change in the laboratory reference system. Thus, to perform statistical analysis over long periods of time and over many different cells (or tandem pairs), we represent the instantaneous traction stress fields in a cell-based (or pair-based) dimensionless coordinate system ($x/a, y/\alpha$). The cell-based (or pair-based) representation involves aligning the longitudinal major axis of the cell (or cell pair) with the horizontal axis, the cell's (or cell pair's) front always pointing in the

positive direction (Figures 1 A-2, A-3, B-2, and B-3), and rescaling all the length dimensions with the half cell (or cell-pair) length, a. The centroid of each cell (or cell-pair) (x_c, y_c) is positioned at the origin of the cell-based (or pair-based) coordinate system. Details of the specific coordinate system can be found elsewhere (del Álamo *et al.*, 2007; Alonso-Latorre, 2010).

We used conditional statistics to characterize the average traction stresses exerted by the different cell lines during the four phases of their motility cycle. The phase-average stress maps were calculated from instantaneous maps of traction stresses after arranging the experimental time-lapse data series by phases. The sorting procedure is based on conditional statistics applied to the time record of the total strain energy, $U_s(t)$ of either the single cell or the cell pair. First, we manually selected the peaks and valleys of each strain energy time record. Then, a computer algorithm automatically divided each cycle of $U_s(t)$ into four phases: phase 1, protrusion (when $U_s(t)$ is increasing); phase 2, contraction (when $U_s(t)$ is maximal); phase 3, retraction (when the $U_s(t)$ is decreasing); and phase 4, relaxation (when $U_s(t)$ is at a local minimum). This previously described algorithm (Meili *et al.*, 2010), worked by applying the following adaptive threshold on U_s (t):

$$Phase(t) =$$

$$\begin{cases} 1\ if\ \alpha(\mathrm{Us_{max}} - \mathrm{Us_{min}}) < \mathrm{Us(t)} - \lambda_{\mathrm{min}} < (1-\alpha)(\mathrm{Us_{max}} - \mathrm{Us_{min}}) and\ \mathrm{t_{min}} < t < t_{\ max}, \\ 2\ if\ |\mathrm{Us_{max}} - \mathrm{Us_{min}}| < \alpha|\mathrm{Us_{max}} - \mathrm{Us_{min}}|, \\ 3\ if\ (\mathrm{Us_{max}} - \mathrm{Us_{min}}) < \mathrm{Us(t)} - \mathrm{Us_{min}} < (1-\alpha)(\mathrm{Us_{max}} - \mathrm{Us_{min}}) and\ \mathrm{t_{max}} < t < t_{\ min}, \\ 4\ if\ |\mathrm{Us(t)} - \mathrm{Us_{min}}| < \alpha(\mathrm{Us_{max}} - \mathrm{Us_{min}}) \end{cases} \quad (15)$$

where t_{min} and t_{max} are the instants of time associated with the nearest local minimum and maximum of U_s (t) and $\mathrm{Us}_{min} = \mathrm{Us(t_{min})}$ and $\mathrm{Us}_{max} = \mathrm{Us(t_{max})}$. Once a phase had been assigned to each time point of our time-lapse experiments, we calculated the average maps of traction stresses based on the conditions that $Phase(t)$ = 1,…4. The threshold needs to be $0 < \alpha < 0.5$ to avoid overlap of adjacent phases and was set to $\alpha = 0.2$. The selection of a threshold for separating the motility cycle into stages was shown to have a negligible effect on the phase-averaged traction maps (Meili *et al.*, 2010).

Analysis of the dynamics of the leading cell's front TA

At each time point, we estimated the position of the minimum value of the axial traction tension T_x at the half front of the tandem pair (blue indicates negative traction tension) by calculating the center of gravity of the fourth power of the negative axial traction tension at the front half of the pair. The resulting time record of the position represents the trajectories of the front TA of the leading cell (Figure 5A). In a similar manner, one could find the trajectory of any TA (the back TA of the leading cell or front TA of trailing cell) providing that the TAs are concentrated in specific areas and are not diffuse. This trajectory of the front TA was smoothed out using a triangular convolution kernel and its time derivative was calculated using a second-order finite difference scheme. This time derivative represents the speed of the frontal (V_F) TA of the leading cell. The mean speed of the cell pair centroid was obtained ($<V_{CM}>$) using the same numerical procedures, and we normalized V_F with $<V_{CM}>$. The magnitude of the normalized speed, $V_F/<V_{CM}>$, was used to determine the front TA's dynamics. When V_F is near zero, it means that the front TA remains stationary (fixed in space). The spikes in this signal are associated with discontinuities in the trajectories of the front TA and thus indicate the establishment of a new TA at the front of the leading cell of the tandem pair (Bastounis *et al.*, 2014).

Using the axial tension kymographs and the calculated values of the normalized speeds of TAs, we established a semi-automatic criterion to identify whether a TA is stable or not. We assumed that normalized TA speeds < 0.5 suggest stationary TA sites. Intermediate normalized speeds between 0.5 and 1 are associated with more diffused, occasionally multiple and temporally dynamic TAs. Finally, normalized speeds >1 are associated with spikes in the signals caused by the appearance or disappearance of TAs. Points between spikes are counted and if the majority have normalized speeds <0.5 the corresponding TA is considered stationary, whereas if the majority have normalized speeds between 0.5 and 1 the corresponding TA is classified as dynamic.

Calculation of the periods of oscillation of different motility time records

We applied wave analysis to measure the dominant period of oscillations of various motility-related time records that we found to be quasi-periodic (Figure 4 C). First, we obtained an initial estimate of the main period, T_0, of these records from the peaks in their autocorrelation functions. Second, we determined the period of the

cycle, T, by fitting the time records to a sinusoidal function of the form: $f(t) = \alpha \sin(\frac{2t}{T} + \varphi)$ in a nonlinear, least squares sense. Because secular fluctuations can shift the detected periods to spurious, long values not related to the changes in cell length associated with the motility cycle, the period *T* was constrained using the initial estimate between $T_0/2$ and $2T_0$. We consistently observed that the best fit resulted from a sine function of a frequency similar to the one determined initially through the autocorrelation function. The value of coefficient α was independently set equal to the absolute maximum of the normalized time record, and its value did not affect the estimation of T. The value of the coefficient φ was not constrained.

Average stress maps during the establishment of front TAs

To gain insight into what happens before and after the establishment of a TA at the front of a pair's leading cell, we identified these events by tracking the spikes in the speed of the location of minimum tension at the front half of the tandem pair (V_F). That allowed us to capture the TA dynamics of the trailing cell as well and assess whether both cells establish their front TA concurrently or not and if not what is the time delay involved. Since wild-type cells predominantly move by keeping their TAs stationary in space (Bastounis *et al.*, 2014), each spike of $V_F/\langle V_{CM} \rangle$ corresponds to the establishment of a new TA at the front of the leading cell (Figure 5 A-B). Since we are interested to compare the dynamics of the front TA of both the leading and trailing cells we discarded the spikes during which the pair was employing Mode 2 and therefore the trailing cell had no front TA. Using the remaining spikes (see red circles in Figure 5B), we compiled average maps of the axial component of the stresses for a number of wild-type tandem pairs 4, 8, 12, and 16 s before and after these spikes emerged. Knowing that at t = 0 a new front TA is established at the front of the pairs' leading cell we were able to precisely assess the time delay in the establishment of the new front TA of the trailing cell.

Calculation of number of aligned and nonaligned pairs formed per hour on different substrata

To quantify the number of pairs formed by different strains and under different substratum coatings we calculated the percentage of cells forming tandem pairs per hour. In order to do this we calculated the total time

of the tandem pairs in each experiment and divided it by the total number of cells multiplied by the time of the recording. In this way we obtained the total percentage of cells forming tandem pairs. By dividing this by the time we obtained the percentage of cells forming tandem pairs per hour. We also measured the time that cell pairs remained together and calculated the statistics of these times for wild-type and *dscA*$^{-}$ cells moving on collagen I-coated and DiscI-coated substrata.

SUPPLEMENTAL REFERENCES

Alonso-Latorre, B. (2010). Force and shape coordination in amoeboid cell motility, University of California, San Diego, PQDT.

Bastounis, E., Meili, R., Alonso-Latorre, B., del Álamo, J., Lasheras, J., and Firtel, R. (2011). The SCAR/WAVE complex is necessary for proper regulation of traction stresses during amoeboid motility. Mol Biol Cell *21*, 3995–4003.

Bastounis, E., Meili, R., Álvarez-González, B., Francois, J., del Álamo, J.C., Firtel, R.A., and Lasheras, J.C. (2014). Both contractile axial and lateral traction force dynamics drive amoeboid cell motility. The Journal of Cell Biology *204*, 1045-1061.

Butler, J.P., Tolic-Norrelykke, I.M., Fabry, B., and Fredberg, J.J. (2002). Traction fields, moments, and strain energy that cells exert on their surroundings. American Journal of Physiology-Cell Physiology *282*, C595-C605.

del Álamo, J.C., Meili, R., Alonso-Latorre, B., Rodríguez-Rodríguez, J., Aliseda, A., Firtel, R.A., and Lasheras, J.C. (2007). Spatio-temporal analysis of eukaryotic cell motility by improved force cytometry. Proc. Nat. Acad. Sci. *104*, 13343-13348.

Engler, A., Bacakova, L., Newman, C., Hategan, A., Griffin, M., and Discher, D. (2004). Substrate compliance versus ligand density in cell on gel responses. Biophys J *86*, 617-628.

Frey, M.T., Engler, A.J., Discher, D.E., Lee, J., and Wang, Y.L. (2007). Microscopic methods for measuring the elasticity of gel substrates for cell culture: microspheres, microindenters, and atomic force microscopy. *Meth. Cell Biol. 83*, 47-65.

Gui, L., and Wereley, S.T. (2002). A correlation-based continuous window-shift technique to reduce the peak-locking effect in digital PIV image evaluation. Exp. Fluids *32*, 506-517.

Keer, L.M. (1964). Stress Distribution at the Edge of an Equilibrium Crack. J. Mech. Physics Solids *12*, 149-163.

Li, Y., Hu, Z., and Li, C. (1993). New method for measuring Poisson's ratio in polymer gels. J. Appl. Polymer Sci., 1107-1111.

Maruthamuthu, V., Sabass, B., Schwarz, U.S., and Gardel, M.L. (2011). Cell-ECM traction force modulates endogenous tension at cell–cell contacts. Proceedings of the National Academy of Sciences *108*, 4708-4713.

Meili, R., Alonso-Latorre, B., Álamo, J.C.d., Firtel, R.A., and Lasheras, J.C. (2010). Myosin II is essential for the spatiotemporal organization of traction forces during cell motility. *Mol. Biol. C*ell *21*, 405-417.

Meili, R., Ellsworth, C., Lee, S., Reddy, T.B., Ma, H., and Firtel, R.A. (1999). Chemoattractant-mediated transient activation and membrane localization of Akt/PKB is required for efficient chemotaxis to cAMP in Dictyostelium. EMBO J *18*, 2092-2105.

Riedl, J., Crevenna, A.H., Kessenbrock, K., Yu, J.H., Neukirchen, D., Bista, M., Bradke, F., Jenne, D., Holak, T.A., Werb, Z., Sixt, M., and Wedlich-Soldner, R. (2008). Lifeact: a versatile marker to visualize F-actin. Nat Methods *5*, 605-607.

Wang, Y.L., and Pelham, R.L. (1998). Preparation of a flexible, porous polyacrylamide substrate for mechanical studies of cultured cells. *Meth. Enzym*. *298*, 489-496.

Willert, C.E., and Gharib, M. (1991). Digital particle image velocimetry. *Exper. in Fluids 10*, 181-193.